Journal of Power Sources 246 (2014) 587–595

Contents lists available at ScienceDirect

Journal of Power Sources

journal homepage: www.elsevier.com/locate/jpowsour

Carbon nanowires@ultrathin SnO_2 nanosheets@carbon composite and its lithium storage properties

Qinghua Tian [a], Zhengxi Zhang [a], Jizhang Chen [a], Li Yang [a,*], Shin-ichi Hirano [b]

[a] School of Chemistry and Chemical Engineering, Shanghai Jiao Tong University, Shanghai 200240, PR China
[b] Hirano Institute for Materials Innovation, Shanghai Jiao Tong University, Shanghai 200240, PR China

HIGHLIGHTS

- We prepared a new morphological nanostructure of composite: CNWs@ ultrathin SnO_2 NSs@C composite.
- The coaxial nanocable-like structure made the composite to have sufficient physical buffer ability.
- The composite exhibited good results in performance of capacity and cycling.

GRAPHICAL ABSTRACT

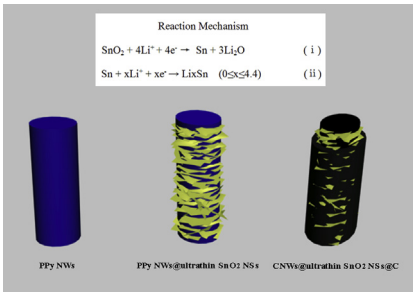

ARTICLE INFO

Article history:
Received 1 July 2013
Received in revised form
19 July 2013
Accepted 3 August 2013
Available online 13 August 2013

Keywords:
Lithium-ion batteries
Anode materials
Ultrathin tin dioxide nanosheets
Coaxial nanocable

ABSTRACT

In this work, a new morphological nanostructure of the CNWs@ultrathin SnO_2 NSs@C composite has been successfully fabricated, realizing the integration of two-dimensional ultrathin SnO_2 NSs and one-dimensional CNWs. The nanosized ultrathin SnO_2 NSs (thickness of ca. 1–3 nm) are uniformly distributed between one dimension CNWs core and C shell, as confirmed by XRD, SEM, TEM and HRTEM characterizations. When tested as potential anode materials for LIBs, the as-prepared coaxial nanocable-like CNWs@ultrathin SnO_2 NSs@C composite exhibits outstanding reversible capacity for lithium storage (695 mAh g^{-1} after 40 cycles at 160 mA g^{-1}, 651 and 618 mAh g^{-1} after 80 cycles at 400 and 800 mA g^{-1}, respectively). This intriguing architecture, which integrates both electronic conductivity and buffering matrix design strategies, contributing to enhanced lithium storage performance.

1. Introduction

With advantages such as high energy density, high safety, low cost, and long lifespan, rechargeable Lithium-ion batteries (LIBs) have attracted great research interest worldwide [1,2]. Recently, LIBs are considered as the most promising energy storage technologies for electrical vehicles and renewable energy such as wind and solar [3–5]. However, current LIBs predominantly use graphite as anode materials, which cannot meet the pressing need for powering electric vehicles (EVs) or hybrid electric vehicles (HEVs) energy storage requirements due to the low theoretical capacity of around 372 mAh g^{-1} [6]. Therefore, it is highly desirable to develop alternative anode materials to meet the need for next-generation LIBs.

SnO_2 has been considered as one of the most promising candidates for anode materials due to its high theoretical capacity of 782 mAh g^{-1}, low toxicity, high abundance and safe working potential [7–9]. Unfortunately, there are two main drawbacks: one is huge volume change of SnO_2 during discharge/charge process, which eventually causes the aggregation and pulverization of SnO_2

* Corresponding author. Tel.: +86 21 54748917; fax: +86 21 54741297.
E-mail address: liyangce@sjtu.edu.cn (L. Yang).

0378-7753/$ – see front matter © 2013 Elsevier B.V. All rights reserved.
http://dx.doi.org/10.1016/j.jpowsour.2013.08.009

with fast capacity fading; the other is poor electronic conductivity of SnO_2, both factors severely hamper the practical usage of the SnO_2 anode for LIBs. To overcome this issue, various SnO_2 nanostructures with large surface area and high surface-to-volume ratio, such as ultrathin nanosheets [10], nanosheets assembled hollow spheres [11], nanowires [12], nanotube arrays [13], nanorods [14], and so forth, have been employed to reduce the absolute volume expansion of tin dioxide. However, considerable capacity fading still exists upon cycling due to the breaking down, aggregation and pulverization of these SnO_2 nanostructures [9]. Another effective way to solve the above-mentioned problems is to design composites with SnO_2 and carbon nanomaterials, which not only improve the conductivity but also accommodate the volume change of SnO_2 during cycles [15,16]. For example, Wu et al. synthesized CNTs@SnO_2@C coaxial nanocables with higher lithium storage capacities and better cycling performance [9]. Zhao et al. prepared SWNTS@SnO_2@PPy coaxial nanocables with greatly improving the capacity [7]. Ding et al. prepared SnO_2 nanosheets grown on graphene sheets with enhanced lithium storage properties [17]. Therefore, carbon has been considered to be a very promising choice as buffering matrix to prevent the broken of SnO_2-based hybrid nanostructures during cycling. However, these means alone only have limited improvement in lithium storage performance of SnO_2-based hybrid nanostructures. Thus, it still exist a huge potential to synthesize and design SnO_2-based hybrid nanostructures with better lithium storage performance.

Herein, we synthesized a new morphological nanostructure of composite, namely carbon nanowires@ultrathin SnO_2 nanosheets@carbon (CNWs@ultrathin SnO_2 NSs@C) composite. The ultrathin SnO_2 nanosheets (SnO_2 NSs) firstly grow on the polypyrrole nanowires (PPy NWs) backbone by facile tin dichloride dihydrate hydrothermal method. Followed by the carbon coating through glucose hydrothermal process and subsequent carbonization approach, the CNWs@ultrathin SnO_2 NSs@C composite was obtained. It is worth mentioning that the PPy NWs were transformed into CNWs during the carbonization process, avoiding specially preparation process of CNWs. The fabrication process is illustrated in Fig. 1. It should be pointed out that PPy is firstly used as CNWs precursor to ultrathin SnO_2 NSs, and the formation of nanosheet-like structures from nonlayered SnO_2 is still extremely challenging. To our knowledge, SnO_2-based composites with such morphology and good lithium storage properties have never been reported before.

2. Experimental section

2.1. Synthesis of the CNWs@ultrathin SnO_2 NSs@C composite

All chemicals were analytical grade and used without further purification.

Preparation of the polypyrrole nanowires@ultrathin SnO_2 NSs (PPy NWs@ultrathin SnO_2 NSs) composite: in a typical experiment, 200 μL of pyrrole (99.7%, Aldrich) was added into 100 mL deionized water containing 60 mg cetyl trimethyl ammonium bromide (CTAB). After stirred for 1 h, 20 mL 0.26 M ammonium persulfate aqueous solution was slowly dropped into above solution. The polymerization process was kept under stirring for 4 h at room temperature. After polymerization process finished, the solution became black suspension. Then 30 mL of the suspension was added into 30 mL ethanol and mixed well. Afterward, 0.12 g tin dichloride dehydrate (AR, Aldrich) was added to above mixture of suspension and ethanol. After stirred for 30 min, followed by the addition of 1.68 g ammonium hydroxide (25–28 wt %). This suspension was transferred into a 100 mL teflon-line stainless autoclave after stirred for 10 min, and then placed in an oven at 120 °C for 6 h. The autoclave used an ice-water bath to rapid cooling after the reaction finished. After that, PPy NWs@ultrathin SnO_2 NSs composite was obtained by centrifugation, washed with deionized water and ethanol thoroughly, and dried in an oven at 60 °C overnight. Pure ultrathin SnO_2 NSs were also synthesized under the same conditions but without adding PPy NWs and CTAB surfactants reported in Ref. [10].

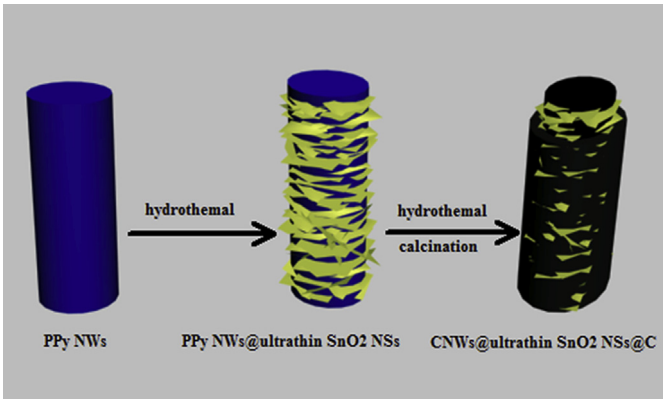

Fig. 1. Schematic illustration of the fabrication process of CNWs@ultrathin SnO_2 NSs@C composite.

Preparation of the CNWs@ultrathin SnO_2 NSs@C composite: CNWs@ultrathin SnO_2 NSs@C composite was synthesized by a modified approach that was similar to reference [9]. Briefly, 100 mg PPy NWs@ultrathin SnO_2 NSs composite was dispersed in 60 mL mixed solvent of 3 M D-glucose aqueous and ethanol with the volume ratio being 1:1. After sonication for 30 min, the suspension was transferred into a 100 mL Teflon-lined stainless autoclave, sealed, and maintained at 190 °C for 4 h. After the reaction was finished, the resulting black solid products were collected by centrifugation and washed with distilled water and ethanol thoroughly, and then dried in a vacuum oven at 60 °C overnight. Finally, the black products were kept in a tube furnace at 500 °C for 3 h under Ar at a ramping rate of 0.5 °C min^{-1}, the CNWs@ultrathin SnO_2 NSs@C composite was obtained. The CNWs@SnO_2 nanoparticles (NPs)@C composite was also synthesized under the same conditions but using PPy@SnO_2 NPs to replace PPy@SnO_2 NSs. And the PPy@SnO_2 NPs composite was synthesized under the same conditions as the PPy@ultrathin SnO_2 NSs but without using an ice-water bath to rapid cooling.

2.2. Structure and electrochemical characterization

The morphology and microstructure of the products were obtained using field emission scanning electron microscopy (FE-SEM, JEOL JSM-7401F), high resolution transmission electron microscopy (HRTEM, JEOL JEM-2010) and transmission electron microscopy (TEM, JEOL JEM-2010) with an energy dispersive X-ray spectrometer (EDX) and a selected-area electron diffraction pattern (SAED). The composition and crystal structure were characterized by X-ray diffraction measurement (XRD, Rigaku, D/max-Rbusing Cu Kα radiation). The SnO_2 content was tested by thermogravimetric analysis (TGA, SDT Q600 V8.2 Bulid 100).

Electrochemical measurements were performed using 2016-type coin cells assembled in an argon-filled glove box (German, M. Braun Co., $[O_2] < 1$ ppm, $[H_2O] < 1$ ppm). The working electrodes were composed of the active material (CNWs@ultrathin SnO_2 NSs@C composite), conductive material (acetylene black, AB), and binder (poly-vinyldifluoride, PVDF) in a weight ratio of CNWs@ultrathin SnO_2 NSs@C composite/AB/PVDF = 80:10:10 and pasted on

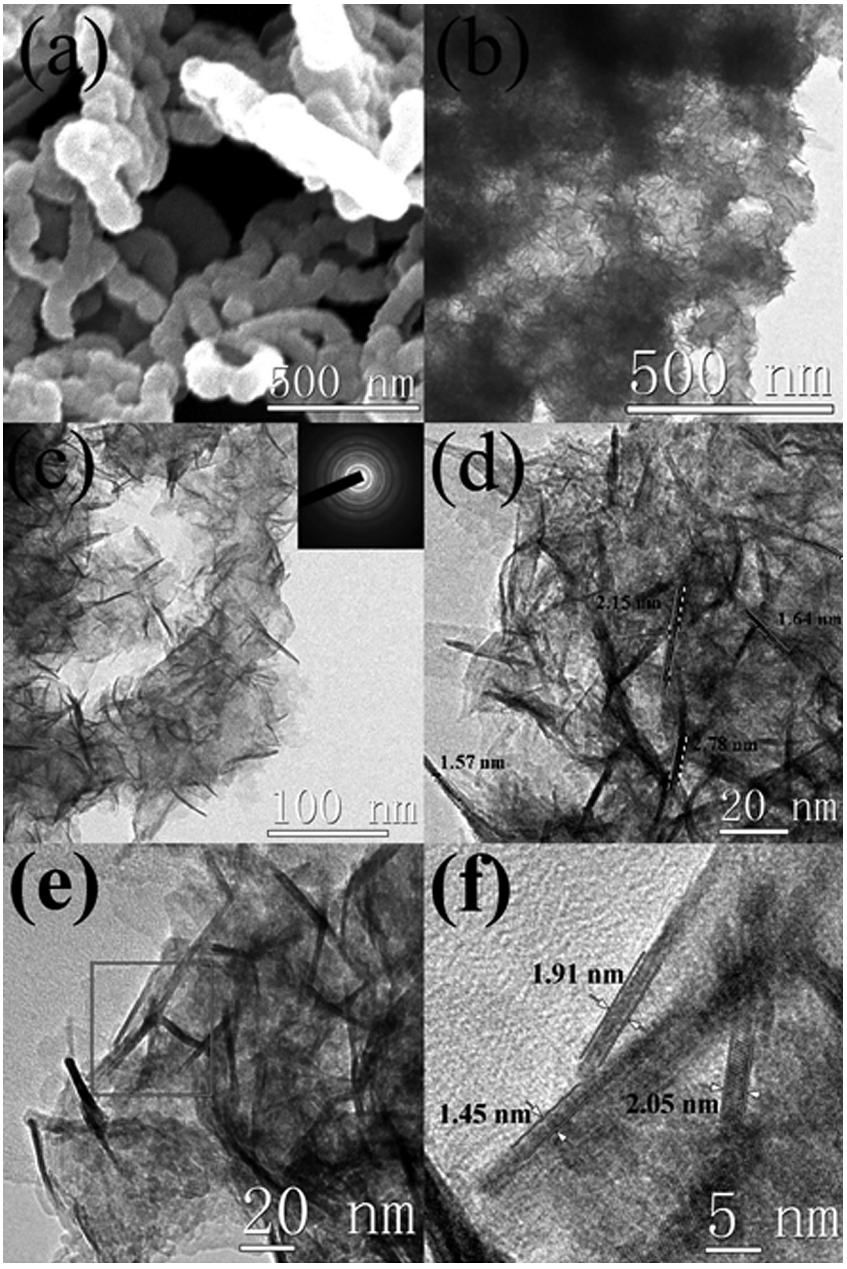

Fig. 2. (a) FESEM image of the PPy NWs; (b, c) TEM image and magnified TEM image of the PPy NWs@ultrathin SnO_2 NSs composite, SAED pattern (inset c) of the ultrathin SnO_2 NSs grew on PPy NWs; (d, e) magnified TEM images of ultrathin SnO_2 NSs; (f) HRTEM image of the ultrathin SnO_2 NSs drawn from the area denoted by a gray square in (e).

Cu foil. Pure lithium foil was used as the counter electrode. A glass fiber (GF/A) from Whatman was used as the separator. The electrolyte consisted of a solution of 1 M $LiPF_6$ in ethylene carbonate and dimethyl carbonate (EC + DMC) (1:1 in volume). The galvanostatic discharge/charge cycles were carried out on a CT2001a cell test instrument (LAND Electronic Co.) over a voltage range of 0.05–3.00 V at room temperature. Cyclic voltammetry (CV) was implemented on a CHI660D electrochemical workstation. Electrochemical impedance spectrum (EIS) measurements were also performed using a CHI660D electrochemical workstation in the frequency rang from 100 kHz to 0.01 Hz with an ac perturbation of 5 mV. For CNWs@ultrathin SnO_2 NSs@C composite working electrode, all the specific capacities reported and current densities used were based on the total weight of CNWs@ultrathin SnO_2 NSs@C composite.

3. Results and discussion

In this CNWs@ultrathin SnO_2 NSs@C composite, CNWs backbone was obtained by using PPy NWs as precursor, which had never been reported for SnO_2 NSs anode materials. Carbon nanotubes (CNTs) usually used as conductive support and backbone for synthesizing SnO_2/carbon composites due to their high conductivity and robust mechanical properties [9,18]. Compared to CNTs, the CNWs obtained from carbonization of PPy NWs precursor have advantages such as simple process of preparation, shape-controlled, lowcost and so on. Thanks to PPy NWs with bigger surface area provided the sites for heterogeneous nucleation of SnO_2, ultrathin SnO_2 NSs grew on the surface of PPy NWs was realized during fabrication process of the composite. The formation mechanism of ultrathin SnO_2 NSs reported in Ref. [10] was that

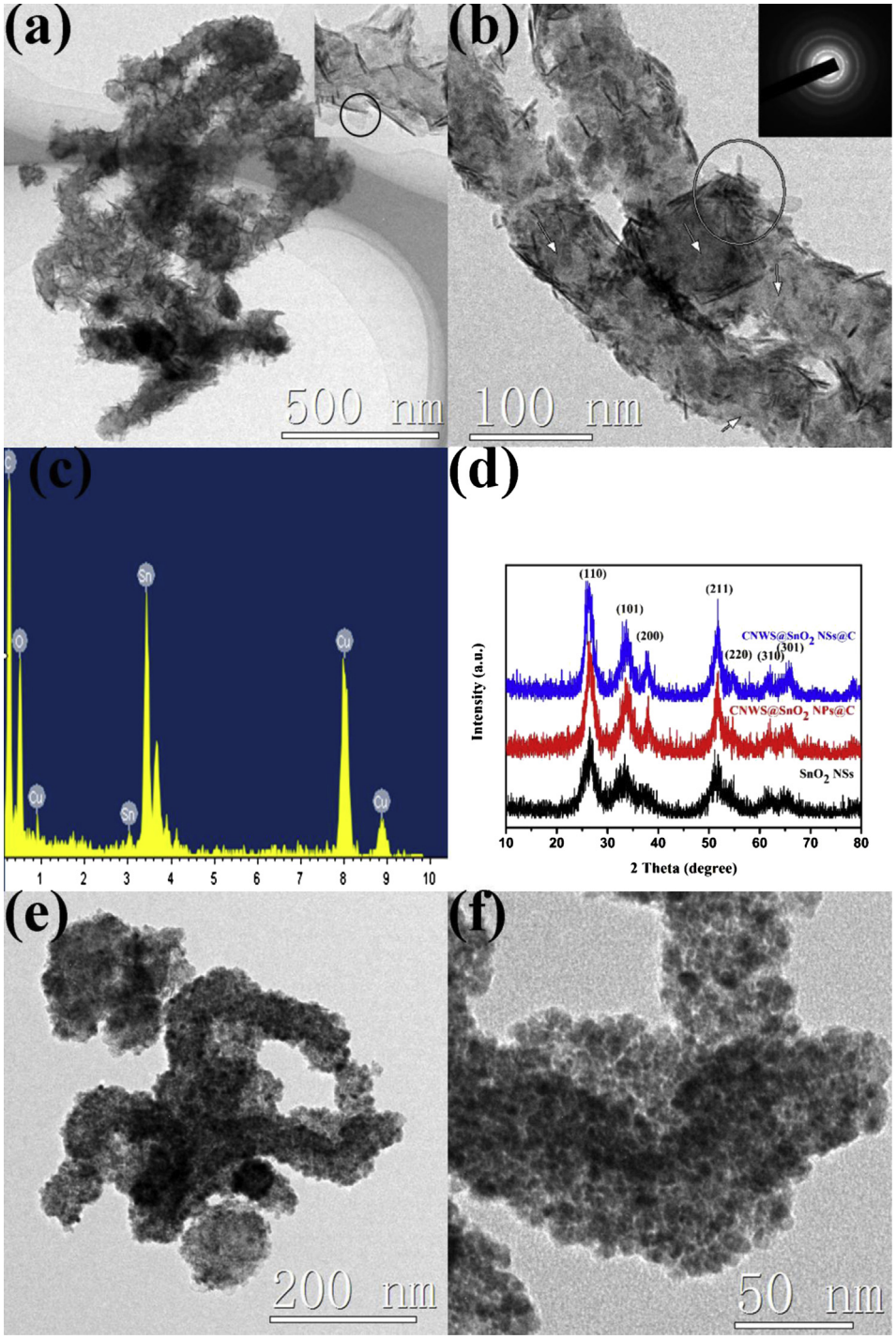

Fig. 3. Morphological, structural, and compositional characterizations of the CNWs@ultrathin SnO_2 NSs@C composite and the CNWs@SnO_2 NPs@C composite: (a) TEM image and magnified TEM image (inset); (b) magnified TEM image, SAED pattern (inset) of the exposed SnO_2 NSs indicated by a gray oval and carbon layer indicated by white arrows; (c) EDS spectrum; (d) XRD pattern; (e, f) TEM images of the CNWs@SnO_2 NPs@C composite with different magnifications.

SnO_2 NSs were assembled by "oriented attachment" of preformed SnO_2 nanoparticles (NPs). This unique architecture would bring high lithium storage and good cycling performance for the CNWs@ultrathin SnO_2 NSs@C composite. We discussed it in the following sections.

The morphology characterizations of PPy NWs, PPy NWs@ultrathin SnO_2 NSs composite and pure ultrathin SnO_2 NSs were carried out using field emission scanning electron microscope (FESEM), high resolution transmission electron microscopy (HRTEM) and transmission electron microscope (TEM). Fig. 2a shows the pristine PPy NWs have curved wires-like shape with a diameter distribution of ca. 100 nm. Fig. 2b, c indicates that the ultrathin SnO_2 NSs uniformly grow on the surface of PPy NWs, where the nanosheet-like structure is formed uniformly throughout the longitudinal axis of the PPy NWs. The light regions suggest planar or bended thin sheets lying on the substrate. Then relatively dark regions indicate that some sheets may either lie aslant, perpendicularly to the substrate or spontaneously convolute

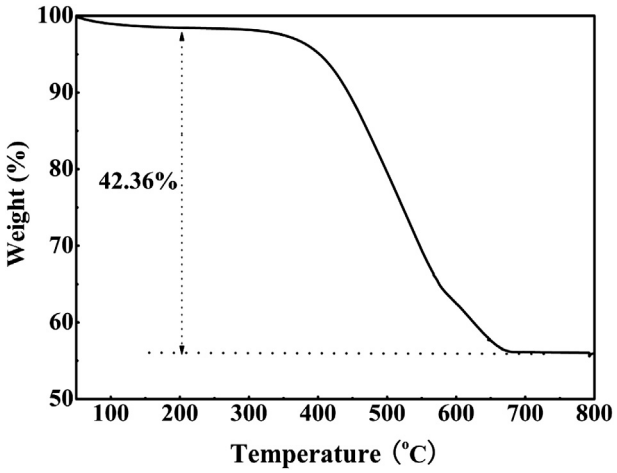

Fig. 4. TGA analysis of the CNWs@ultrathin SnO2 NSs@C composite.

due to minimization of surface energy. The selected-area electron diffraction (SAED) pattern (inset of Fig. 2c) indicates that the SnO_2 NSs reveal polycrystalline in nature, because there are three diffraction rings corresponding to the (110), (101) and (211) planes of polycrystalline SnO_2, respectively. The SnO_2 NSs densely grafted around the PPy NWs backbone shown in Fig. 2c. Moreover, magnified TEM images and HRTEM image indicate that the nanosheets are about 100 nm in width and ca. 1–3 nm in thickness shown in Fig. 2d, e and f, respectively. The XRD pattern of the pure ultrathin SnO_2 NSs (Fig. 3d) indicates it can be indexed to pure rutile SnO_2 (JCPDS card no. 41-1445, SG: P42/mnm. $a_o = 4.738$ Å, $c_o = 3.187$ Å) [19].

Fig. 3 displays the morphological, structural, and compositional characterizations of CNWs@ultrathin SnO_2 NSs@C composite. As can be seen from Fig. 3a, b that the 1 D nanostructure is preserved after the PPy NWs@ultrathin SnO_2 NSs coated by carbon layer, as well as the ultrathin SnO_2 NSs morphology is maintained and sandwiched between CNWs and carbon layer. The relatively dark lines are the top views of the edges of SnO_2 NSs "standing" upright on the CNWs backbone shown in Fig. 3a. Ultrathin SnO_2 NSs with a large width "standing" upright on the CNWs backbone and the carbon layer is too thin (indicated by white arrows in Fig. 3b) to coat the SnO_2 NSs completely. However, the thin carbon layer is in favor of improving lithium storage of SnO_2/carbon composite [9]. It can be seen that a single SnO_2 nanosheet is observed and indicated by a black circle shown in inset of Fig. 3a. In addition, the exposed SnO_2 NSs are indicated by a gray oval in Fig. 3b further confirmed by the SAED pattern (inset of Fig. 3b).

The crystallographic structure of the CNWs@ultrathin SnO_2 NSs@C composite was further characterized by using X-ray diffraction (XRD) shown in Fig. 3d. As observed, all of the diffraction peaks of CNWs@ultrathin SnO_2 NSs@C composite (Fig. 3d, pattern top) can be indexed to pure rutile SnO_2 (JCPDS card no. 41-1445, SG: P42/mnm. $a_o = 4.738$ Å, $c_o = 3.187$ Å) [19]. Additionally, the carbon is hard to trace in XRD analysis, which suggests the carbon coating are amorphous carbon. The broad peaks with low intensities in these samples indicate the small size of the SnO_2 shown in Fig. 3d. Compared to pure SnO_2 NSs, the peaks intensities of the two composites increased after carbonization owing to the increase of the crystallinity of SnO_2. Fig. 3c is the EDS spectrum taken from a single CNWs@ultrathin SnO_2 NSs@C composite (Fig. 3b). As can be seen from this spectrum, the strong peaks for C, Sn and O elements are expected from the CNWs, carbon layer and SnO_2 NSs, respectively. Then the Cu peaks come from micro-grid used as the sample stage in TEM measurements. The results discussed above confirm that we have successfully obtained the CNWs@ultrathin SnO_2 NSs@C composite. For comparing the electrochemical properties of CNWs@SnO_2 NSs@C and CNWs@SnO_2 nanoparticles (NPs)@C composite, we also prepared the CNWs@SnO_2 NPs@C composite displayed in Fig. 3e, f. It is clearly seen that SnO_2 NPs are uniformly monodispersed on CNWs without SnO_2 NSs. The CNWs@SnO_2 NPs@C composite was also investigated by XRD (Fig. 3d), and can be indexed to pure rutile SnO_2 (JCPDS card no. 41-1445, SG: P42/mnm. $a_o = 4.738$ Å, $c_o = 3.187$ Å) [19].

The weight fraction of SnO_2 in the CNWs@ultrathin SnO_2 NSs@C composite was determined by thermogravimetric analysis (TGA), with the results shown in Fig. 4. As observed, the curve of the CNWs@ultrathin SnO2 NSs@C composite displays two distinct regions of weight loss. The initial weight loss between 200 and 600 °C is mainly due to the removal of carbon layer [20], while the weight loss in the second region (600–800 °C) could be attributed to the combustion of residual carbon layer and CNWs, since CNWs is more thermally stable than carbon layer. After reaching 800 °C, the CNWs@ultrathin SnO_2 NSs@C composite shows a total weight loss of 42.36%, determining the SnO_2 contents are about 57.64% by weight.

The electrochemical properties of the CNWs@ultrathin SnO_2 NSs@C composite as potential anode materials for lithium-ion batteries were investigated. The possible reaction mechanism of SnO_2/Li cell is proposed as follows [21,22]:

$$SnO_2 + 4Li^+ + 4e^- \rightarrow Sn + 3Li_2O \quad (1)$$

$$Sn + xLi^+ + x\,e^- \rightarrow Li_xSn\ (0 \le x \le 4.4) \quad (2)$$

Fig. 5a shows the initial five CV curves of the CNWs@ultrathin SnO_2 NSs@C composite at a scan of 0.5 mV s^{-1} from 0.0 to 3.0 V. There is a broad reduction peak near 0.87 V in the first cathodic scan, which is attributed to the formation of a solid electrolyte interface (SEI) layer and the conversion of SnO_2 to metallic Sn. This peak shows a significantly drop in current after the first cycle correspond to the conversion reaction only. As can be seen from Fig. 5a that two characteristic pairs of redox peaks are clearly observed in the CV curves, locating at 0.03 and 0.63 V and 0.9 and 1.29 V, respectively. Specifically, it should be noted that a broad cathodic peak (0.7–1.3 V) and a corresponding anodic peak (1.0–1.5 V) still exist during the fifth cycle, suggesting partial reversibility of reaction (1). Note here, according to Wang et al. previously reported, it has indeed been found that the partial electrochemical reversibility of Li_2O is able to activate when applied nanosized particles (10–20 nm) with large surface areas [10,23]. Thus, we believe that the observed partial reversibility of reaction (1) is due to the ultrathin thickness of SnO_2 NSs. Fig. 5b shows the charge–discharge voltage profile of the CNWs@ultrathin SnO_2 NSs@C composite measured at a constant current density of 160 mA g^{-1}. In agreement with its CV behavior, two poorly defined plateau regions can be identified in the first discharge process, and it gives a very high discharge capacity of 1727 mAh g^{-1} (throughout this work, the specific capacity of CNWs@ultrathin SnO_2 NSs@C composite calculated based on the total mass of CNWs@ultrathin SnO_2 NSs@C composite). And the following charge process features a charge capacity of 1061 mAh g^{-1}, distributing to a relatively higher Coulombic efficiency of 61.4% as compared to other composites (in this work, the specific capacities of all reported composites calculated based on their total mass) [24,25], which is owing to its unique nanostructure. As well known, large initial capacity loss is common for SnO_2 materials, which is mainly ascribing to the first irreversible reactions, such as the irreversible formation of the SEI layer, electrolyte decomposition and so on. The discharge and

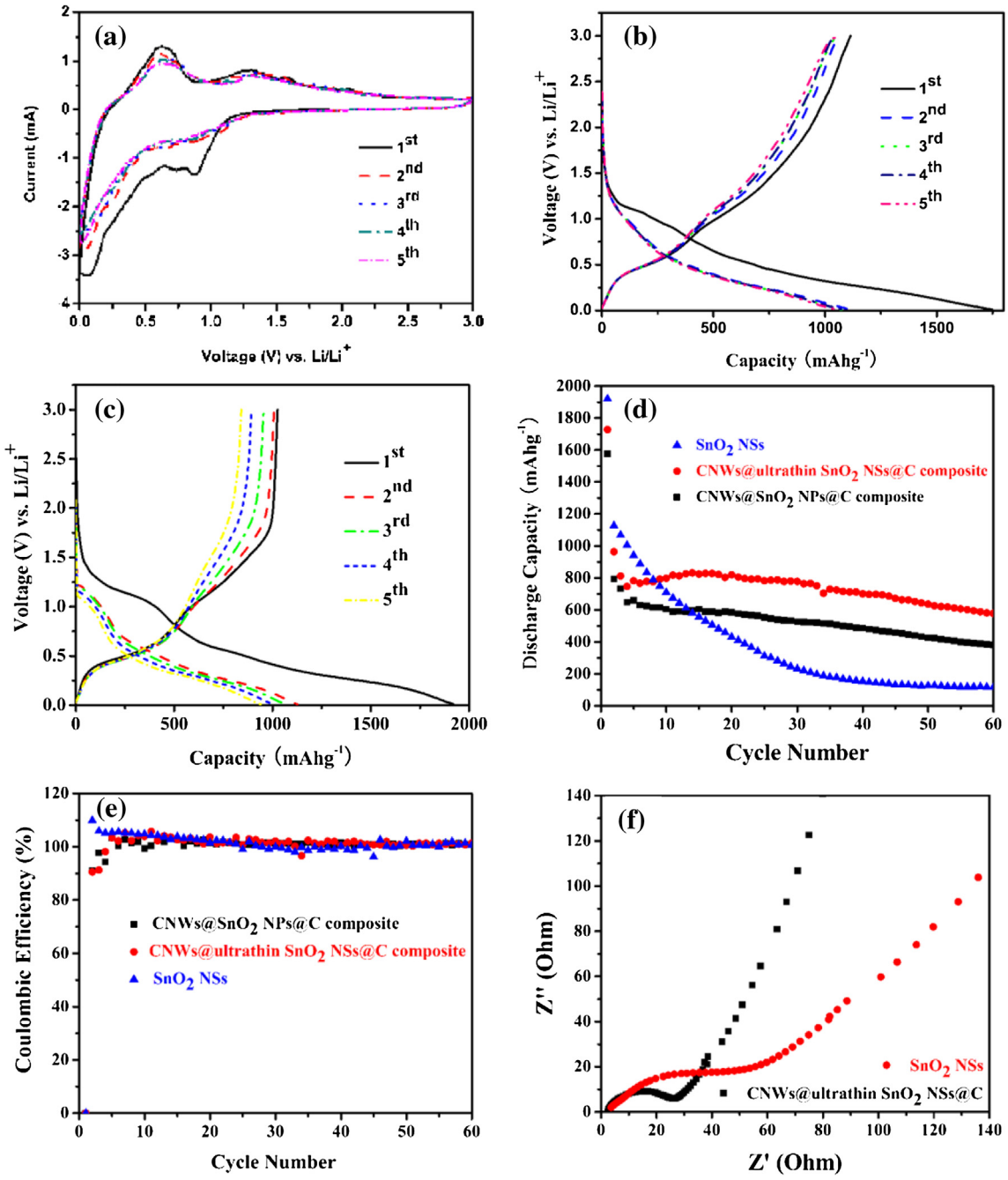

Fig. 5. Electrochemical characterizations of the CNWs@ultrathin SnO_2 NSs@C composite, CNWs@SnO_2 NPs@C composite and SnO_2 NSs: (a) representative CVs of the CNWs@ultrathin SnO_2 NSs@C composite at a scan rate of 0.5 mV s^{-1} between 0.0 V and 3.0 V; (b, c) charge/discharge voltage profiles of the CNWs@ultrathin SnO_2 NSs@C composite and SnO_2 NSs at 160 mA g^{-1}, respectively; (d) comparative cycling performance between different samples at current density of 160 mA g^{-1}; (e) Coulombic efficiencies of the CNWs@ultrathin SnO_2 NSs@C composite, CNWs@SnO_2 NPs@C composite and ultrathin SnO_2 NSs (Coulombic efficiency = Discharge capacity/Charge capacity × 100%); (f) Nyquist plots of the CNWs@ultrathin SnO_2 NSs@C composite and SnO_2 NSs after five charge/discharge cycles.

charge capacities in the second cycle are 963 and 889 mAh g^{-1}, respectively, resulting in an increased efficiency value of 92.3%. Moreover, the efficiency further increases up to 95.9% in the fifth cycle and keeps increasing in the following cycles shown in Fig. 5e. It is worth noting that the charge curves in the following cycles almost overlapped with the first one, further showing a good cycling performance of the CNWs@ultrathin SnO_2 NSs@C composite. In addition, it can be seen that the actual capacity of the CNWs@ultrathin SnO_2 NSs@C composite is clearly than theoretical value (782 mAh g^{-1}) of SnO_2 in the first few cycles. This phenomenon suggests that an electrochemical conversion reaction occurs between Li_2O and metallic Sn ($Li_2O + Sn \leftrightarrow SnO + Li$) during discharge/charge cycles of the CNWs@ultrathin SnO_2 NSs@C composite, and the reversible oxidation of Sn to SnO in this composite increases its initial coulombic efficiency and specific capacity [26]. As well as the ultrathin thickness of SnO_2 NSs of the CNWs@ultrathin SnO_2 NSs@C composite is also beneficial to enhance coulombic efficiency and specific capacity of this composite, owing

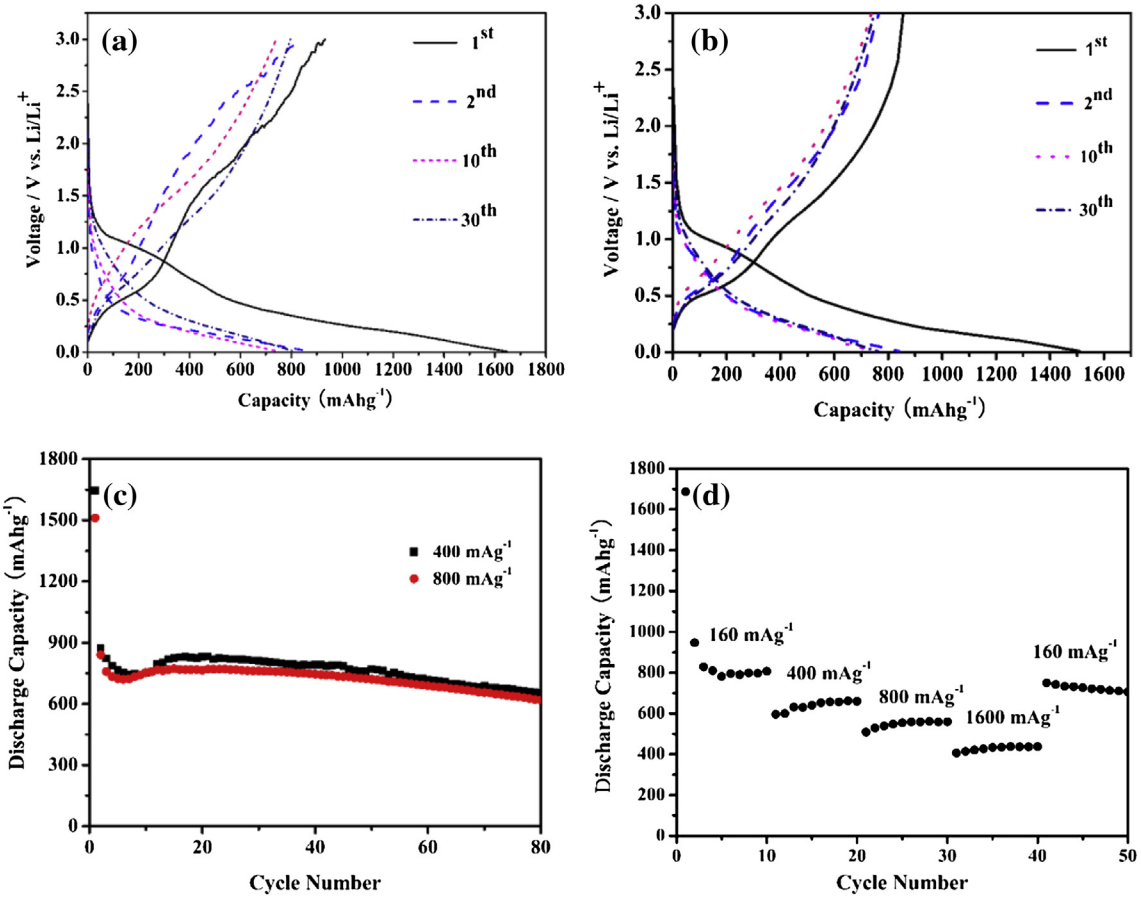

Fig. 6. (a, b) The charge–discharge voltage profiles of the CNWs@ultrathin SnO_2 NSs@C composite at current density of 400 mA g^{-1} and 800 mA g^{-1}, respectively; (c) Cycle performance of the CNWs@ultrathin SnO_2 NSs@C composite in 0.0–3.0 V (vs. Li/Li^+) voltage window at current density of 400 mA g^{-1} and 800 mA g^{-1}, respectively; (d) rate capabilities of the CNWs@ultrathin SnO_2 NSs@C composite.

to the partial electrochemical reversibility of Li_2O is able to activate when applied nanosized particles (10–20 nm) with large surface areas [10,23].

Fig. 5d shows the comparison of cycling performance between CNWs@ultrathin SnO_2 NSs@C composite and SnO_2 NSs between 0.0 and 3.0 V at a current density of 160 mA g^{-1}. It can be seen that the CNWs@ultrathin SnO_2 NSs@C composite demonstrates enhanced cyclic capacity retention over the pure SnO_2 NSs counterpart. The CNWs@ultrathin SnO_2 NSs@C composite delivers a high discharge capacity of 695 mAh g^{-1} after 40 cycles and even can remain at 577 mAh g^{-1} in 60 cycles, compared to 154 and 116 mA h^{-1} for the SnO_2 NSs. Fig. 5c shows that the SnO_2 NSs exhibit a high capacity in first few cycles and deliver an initial discharge capacity of 1920 mAh g^{-1} due to their unique nanosheet-like structure, since the ultrathin nanosheet architecture can provide negligible diffusion time and shortened diffusion path of lithium ions and probably faster phase transitions [10]. In Fig. 5d, however, the SnO_2 NSs with fast capacity fading can be observed during discharge/charge cycles due to their aggregation and pulverization [9]. Then, we also compared the cyclic performance of the CNWs@ultrathin SnO_2 NSs@C composite with CNWs@SnO_2 NPs@C composite shown in Fig. 5d, the CNWs@SnO_2 NPs@C delivers a discharge capacity of 486 mAh g^{-1} after 40 cycles and only remains at 381 mAh g^{-1} in the 60 cycles, indicating the cycling performance of the CNWs@ultrathin SnO_2 NSs@C composite is significantly improved. In addition, we further compared the lithium storage properties with that of similar composites which have been reported, such as the CNTs@SnO_2@C-thin coaxial nanocables [9], SnO_2@PPy nanowires [27] and the one-dimensional SnO_2 NSs@CNT hierarchical structure composite [28]. The CNTs@SnO_2@C-thin coaxial nanocables delivered a discharge capacity of about 450 mAh g^{-1} after 30 cycles at 100 mA g^{-1}, and the initial Coulombic efficiency was 49.3%; The SnO_2@PPy nanowires delivered a discharge capacity of 430 mAh g^{-1} after 20 cycles at 60 mA g^{-1}, and the initial Coulombic efficiency was 39.4%; The one-dimensional SnO_2 NSs@CNT hierarchical structure composite delivered a discharge capacity of 549 mAh g^{-1} after 40 cycles at 160 mA g^{-1}, and the initial Coulombic efficiency was 39.6%. Thus, compared to them, this CNWs@ultrathin SnO_2 NSs@C composite manifest greatly enhanced lithium storage properties and cycling performance, which is mainly due to the unique properties of the ultrathin SnO_2 NSs and the structure of composite. The results suggest that the ultrathin sheets architecture can provide negligible diffusion time and shortened diffusion path of lithium ions and probably faster phase transitions. Moreover, the sandwich-like one-dimensional nanowires structure can also be beneficial to buffer drastic volume changes and preserve the morphology of SnO_2 NSs during the discharge/charge process.

Electrochemical impedance spectroscopy (EIS) measurements were carried out to better demonstrate the effect of carbon (CNWs and carbon coating) on the electronic conductivity of the CNWs@ultrathin SnO_2 NSs@C composite. Fig. 5f shows the Nyquist plots of the CNWs@ultrathin SnO_2 NSs@C composite and the only SnO_2 NSs electrodes after five discharge/charge cycles. Both

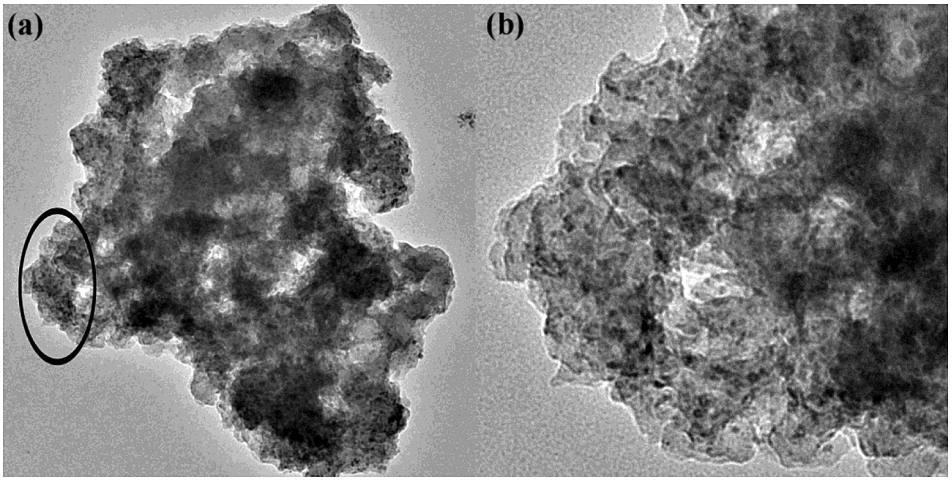

Fig. 7. (a) TEM image of the CNWs@ultrathin SnO2 NSs@C composite after 60 cycles at 160 mA g^{-1}; (b) magnified TEM image of the part of (a) indicated by a black oval.

electrodes exhibit Nyquist plots consisting of a depressed semicircle at high frequency range and an angled straight line in the low frequency range. The diameter of the depressed semicircle is correlated with the electron transfer resistance on the electrode interface, and the angled straight line is related to a diffusion controlled process. Apparently, the CNWs@ultrathin SnO_2 NSs@C composite delivers a much smaller diameter of the high frequency semicircle compared with that of the only SnO_2 NSs electrode, indicating enhanced electron and lithium ion transport [29].

The cycling performance of the CNWs@ultrathin SnO_2 NSs@C composite was also investigated at high current density. Fig. 6a, b shows the discharge/charge voltage profiles of the CNWs@ultrathin SnO_2 NSs@C composite at current density of 400 mA g^{-1} and 800 mA g^{-1}, respectively. As observed from Fig. 6a, b that the sample delivers an initial discharge capacity of 1644 mAh g^{-1} and 1511 mAh g^{-1} at current density of 400 and 800 mA g^{-1}, respectively. The good cycling performance still existed in high current density demonstrated by the almost same trend of discharge curve with first one after several cycles. In Fig. 6c, the as-prepared composite exhibits a reversible capacity of 629 mAh g^{-1} after 80 cycles at a current density of 400 mA g^{-1}, manifesting greatly enhanced lithium storage properties compared to one-dimensional SnO_2 NSs@CNT hierarchical structure composite (420 mAh g^{-1} after 30 cycles at 400 mA g^{-1}) [28] and CNTs@SnO_2@carbon (505 mAh g^{-1} after 60 cycles at 400 mA g^{-1}) [30]. When a higher current density of 800 mA g^{-1} is employed, a reversible capacity of 611 mAh g^{-1} can be still obtained after 80 cycles. The results further demonstrated the good cycling performance of the CNWs@ultrathin SnO_2 NSs@C composite at high current density. The good lithium storage property at high current density attributed to the intimate interactions between CNWs and the ultrathin SnO_2 NSs, which could effectively and rapidly transport electrons between SnO_2 and carbon to the current collector through the highly conducting one-dimensional coaxial nanocable-like structure, and demonstrated by the EIS shown in Fig. 5f. It is interesting to observe from Fig. 6c that the phenomena of the consistent decrease in reversible capacity until to about 6th cycle, then consistent increase with the cycle number to 16th cycle. We speculate that it is mainly owing to the lithium-ion needs more time to permeate and contact with those buried ultrathin SnO_2 nanosheets with larger surface area of the CNWs@ultrathin SnO_2 NSs@C composite.

Fig. 6d illustrates the rate performance of the CNWs@ultrathin SnO_2 NSs@C composite at various current densities from 160 to 1600 mA g^{-1}. The specific capacities of the composite are 806, 659, 559 and 437 mAh g^{-1} when cycles at 160, 400, 800 and 1600 mA g^{-1}, respectively. When back to 160 mA g^{-1}, a capacity of 705 mAh g^{-1} can be restored, indicating the good rate performance and stability of the CNWs@ultrathin SnO_2 NSs@C composite.

To further understand the good electrochemical performance of the CNWs@ultrathin SnO2 NSs@C composite, we decomposed a cell after 60 cycles at a current density of 160 mA^{-1} and characterized the morphology by TEM. As observed from Fig. 7, the curved wires-like morphology is still preserved, and the ultrathin SnO_2 NSs is broken but still existence, showing the good stability of this composite during discharge/charge cycles. Thus, this unique coaxial nanocable-like structure of the CNWs@ultrathin SnO_2 NSs@C composite has two dominating advantages for improving the electrochemical performance. First, ultrathin SnO_2 NSs could provide negligible diffusion time and shortened diffusion path of lithium ions and probably faster phase transitions. Second, the coaxial nanocable-like one-dimensional nanowires structure, with ultrathin SnO_2 NSs uniformly distributed between CNWs and C, could effectively buffer drastic volume changes during the reactions, improve the electronic conductivity, prevent the aggregation of SnO_2, and maintain the good contact between Li_2O and Sn during discharge/charge process, to realize the highly reversible conversion and alloy reaction of SnO_2 during cycling with good stability.

4. Conclusions

In summary, we have successfully prepared CNWs@ultrathin SnO_2 NSs@C composite. CNWs and carbon layer in the resulting composite can effectively prevent the aggregation of SnO_2 NSs sandwiched between them, improve the electronic conductivity and buffer volume change and accommodate structural stress of SnO_2 during electrochemical process. The ultrathin SnO_2 NSs of CNWs@ultrathin SnO_2 NSs@C composite can provide negligible diffusion time and shortened diffusion path of lithium ions, which contributing to enhanced electrochemical properties with high reversible capacities and good cycling performance. When tested as potential anode materials for LIBs, the coaxial nanocable-like CNWs@ultrathin SnO_2 NSs@C composite delivers a high discharge capacity of 695 mAh g^{-1} after 40 cycles at 160 mA g^{-1}. Moreover, it also delivers a reversible capacity of ca. 651 and 618 mAh g^{-1} after 80 cycles at 400 and 800 mA g^{-1}, respectively. Thus, the as-prepared CNWs@ultrathin SnO_2 NSs@C composite exhibits high lithium storage capacities and good cycling performance, which are

largely due to the unique integration of two-dimensional ultrathin SnO_2 NSs and one-dimensional coaxial nanocable-like architecture.

References

[1] M.R. Palacin, Chem. Soc. Rev. 38 (2009) 2565.
[2] B. Scrosati, J. Garche, J. Power Sources 195 (2010) 2419.
[3] H. Shi, J. Barker, M.Y. Saidi, R. Koksbang, L. Morris, J. Power Sources 68 (1997) 291.
[4] Z. Wei, H. Mao, T. Huang, A.S. Yu, J. Power Sources 233 (2013) 50.
[5] F.S. Ke, L. Huang, B.C. Solomon, G.Z. Wei, L.J. Xue, B. Zhang, J.T. Li, X.D. Zhou, S.G. Sun, J. Mater. Chem. 22 (2012) 17511.
[6] Z.H. Wen, G.H. Lu, S. Mao, H. Kim, S.M. Cui, K.H. Yu, X.K. Huang, P.T. Hurley, O. Mao, J.H. Chen, Electrochem. Commun. 29 (2013) 67.
[7] Y. Zhao, J. Li, N. Wang, C.X. Wu, G.F. Dong, L.H. Guan, J. Phys. Chem. C 116 (2012) 18612.
[8] C. Wang, Y. Zhou, M.Y. Ge, X.B. Xu, Z.L. Zhang, J.Z. Jiang, J. Am. Chem. Soc. 132 (2010) 46.
[9] P. Wu, N. Du, H. Zhang, J.X. Yu, D.R. Yang, J. Phys. Chem. C 114 (2010) 22,535–22,538.
[10] C. Wang, G.H. Du, K. Stahl, H.X. Huang, Y.J. Zhong, J.Z. Jiang, J. Phys. Chem. C 116 (2012) 4000–4011.
[11] S.J. Ding, X.W. Lou, Nanoscale 3 (2011) 3586.
[12] J. Pan, X.F. Song, J. Zhang, H. Shen, Q.H. Xiong, J. Phys. Chem. C 115 (2011) 22,225.
[13] J.Z. Wang, N. Du, H. Zhang, J.X. Yu, D.R. Yang, J. Phys. Chem. C 115 (2011) 11,302.
[14] J.P. Liu, Y.Y. Li, X.T. Huang, R.M. Ding, Y.Y. Hu, J. Jiang, L. Liao, J. Mater. Chem. 19 (2009) 1859.
[15] S.M. Paek, E. Yoo, I. Honma, Nano Lett. 9 (2009) 72.
[16] L. Noerochim, J.Z. Wang, S.L. Chou, D. Wexler, H.K. Liu, Carbon 50 (2012) 1289.
[17] S.J. Ding, D.Y. Luan, F.Y.C. Boey, J.S. Chen, X.W. Lou, Chem. Commun. 47 (2011) 7155.
[18] G. Chen, Z.Y. Wang, G.D. Xia, Chem. Mater. 20 (2008) 6951.
[19] S.J. Ding, J.S. Chen, G.G. Qi, X.N. Duan, Z.Y. Wang, E.P. Giannelis, L.A. Archer, X.W. Lou, J. Am. Chem. Soc. 133 (2011) 21–23.
[20] J.S. Chen, Y.L. Cheah, Y.T. Chen, N. Layaprakash, S. Madhavi, H.Y. Yang, X.W. Lou, J. Phys. Chem. C 113 (2009) 20,504.
[21] I.A. Courtney, J.R. Dahn, J. Electrochem. Soc. 144 (1997) 2045–2052.
[22] I.A. Courtney, W.R. Mckinnon, J.R. Dahn, J. Electrochem. Soc. 146 (1999) 59–68.
[23] S.C. Nam, Y.S. Yoon, B.W. Cho, H.S. Chun, K.S. Yun, J. Electrochem. Soc. 148 (2001) A220–A223.
[24] C. Zhong, J.Z. Wang, Z.X. Chen, H.K. Liu, J. Phys. Chem. C 115 (2011) 25,115.
[25] X. Li, X. Meng, J. Liu, D. Geng, Y. Zhang, M.N. Banis, Y. Li, J. Yang, R. Li, X. Sun, Adv. Funct. Mater. 22 (2012) 1647.
[26] X.W. Guo, X.P. Fang, Y. Sun, L.Y. Shen, Z.X. Wang, L.Q. Chen, J. Power Sources 226 (2013) 75–81.
[27] L.F. Cui, J. Shen, F.Y. Cheng, Z.L. Tao, J. Chen, J. Power Sources 196 (2011) 2195–2201.
[28] S.J. Ding, J.S. Chen, X.W. Lou, Adv. Funct. Mater. 21 (2011) 4124.
[29] C.F. Zhang, X. Peng, Z.P. Guo, C.B. Cai, Z.X. Chen, D. Wexler, S.A. Li, H.K. Liu, Carbon 50 (2012) 1897–1903.
[30] S.J. Ding, J.S. Chen, X. w. Lou, Chem. Asian J. 6 (2011) 2278–2281.